ACS OMEGA

http://pubs.acs.org/journal/acsodf

Article

NaCl-Assisted Temperature-Dependent Controllable Growth of Large-Area MoS_2 Crystals Using Confined-Space CVD

Muhammad Suleman, Sohee Lee, Minwook Kim, Van Huy Nguyen, Muhammad Riaz, Naila Nasir, Sunil Kumar, Hyun Min Park, Jongwan Jung, and Yongho Seo*

Cite This: *ACS Omega* 2022, 7, 30074−30086

Read Online

ACCESS | Metrics & More | Article Recommendations | Supporting Information

ABSTRACT: Due to its semiconducting nature, controlled growth of large-area chemical vapor deposition (CVD)-grown two-dimensional (2D) molybdenum disulfide (MoS_2) has a lot of potential applications in photodetectors, sensors, and optoelectronics. Yet the controllable, large-area, and cost-effective growth of highly crystalline MoS_2 remains a challenge. Confined-space CVD is a very promising method for the growth of highly crystalline MoS_2 in a controlled manner. Herein, we report the large-scale growth of MoS_2 with different morphologies using NaCl as a seeding promoter for confined-space CVD. Changes in the morphologies of MoS_2 are reported by variation in the amount of seeding promoter, precursor ratio, and the growth temperature. Furthermore, the properties of the grown MoS_2 are analyzed using optical microscopy, scanning electron microscopy (SEM), Raman spectroscopy, X-ray photoelectron spectroscopy (XPS), energy-dispersive X-ray spectroscopy (EDX), and atomic force microscopy (AFM). The electrical properties of the CVD-grown MoS_2 show promising performance from fabricated field-effect transistors. This work provides new insight into the growth of large-area MoS_2 and opens the way for its various optoelectronic and electronic applications.

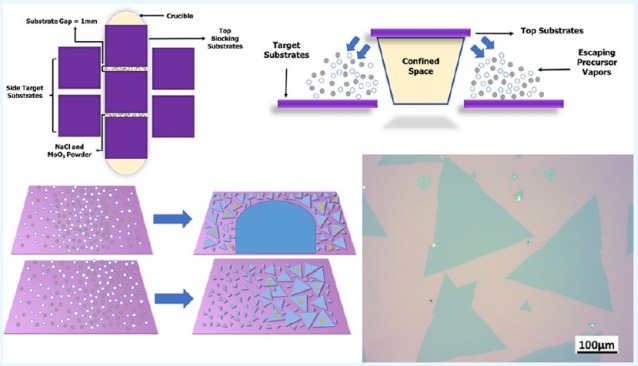

INTRODUCTION

Transition-metal dichalcogenides have gained a lot of popularity in recent years mainly because of the advantages they provide in terms of their usage in field-effect transistors (FETs),[1] photodetectors,[2] photodiodes,[3] solar cells,[4] and phototransistors.[5] The layers of two-dimensional (2D) materials can be ultrathin, and the band gap can be tuned according to the thickness of the layers of the material from monolayer to multilayer.[6−8] MoS_2 is a very promising 2D material because of its outstanding performance in terms of carrier mobility,[9] tunability of excitonic effects,[10] and high current density of monolayer.[11] MoS_2 is also one of the stable 2D materials available which makes its fabrication process easier than other materials.[12] All of these applications of MoS_2 rely heavily on the size, shape, and crystallinity of the crystal. The electronic structure of MoS_2 can be tuned with the thickness of the crystals, which can be used for applications like spin−valley coupling[13] and abundant excitons.[14]

One of the methods of obtaining 2D MoS_2 is mechanical exfoliation, which is not compatible with industrial-scale manufacturing.[15] Therefore, large-scale synthesis of 2D MoS_2 has always been a challenge. Other methods include physical vapor deposition,[16] chemical vapor deposition (CVD),[17] liquid exfoliation,[18] and hydrothermal synthesis.[19] Of all of the mentioned methods, CVD is preferred for the cost-effective growth of highly crystalline and uniform synthesis of 2D MoS_2.[20] Controllable growth of MoS_2 crystals is highly desirable, allowing the control of thickness,[21] shape, and size of the MoS_2 crystals.[22] CVD provides an excellent opportunity for the controllable growth of the MoS_2 crystals as there are several controllable variables which can impact the growth of MoS_2 crystals.[23] Depending on the control method for CVD, various techniques have been established for the controllable growth of MoS_2 crystals. A better understanding of the chemistry inside the CVD chamber such as the precursor ratio, precursor decomposition rate, nucleation, and diffusion provides the basis for establishing control over the growth of MoS_2 crystals.[24]

Seeding promoters have been extensively used for the highly crystalline growth of MoS_2.[25] Studies have been conducted on the role of alkali metal−based salts in the growth of transition metal dichalcogenide (TMDC) materials, and it has been observed that these salts act as seeding promoters having a

Received: May 18, 2022
Accepted: August 10, 2022
Published: August 22, 2022

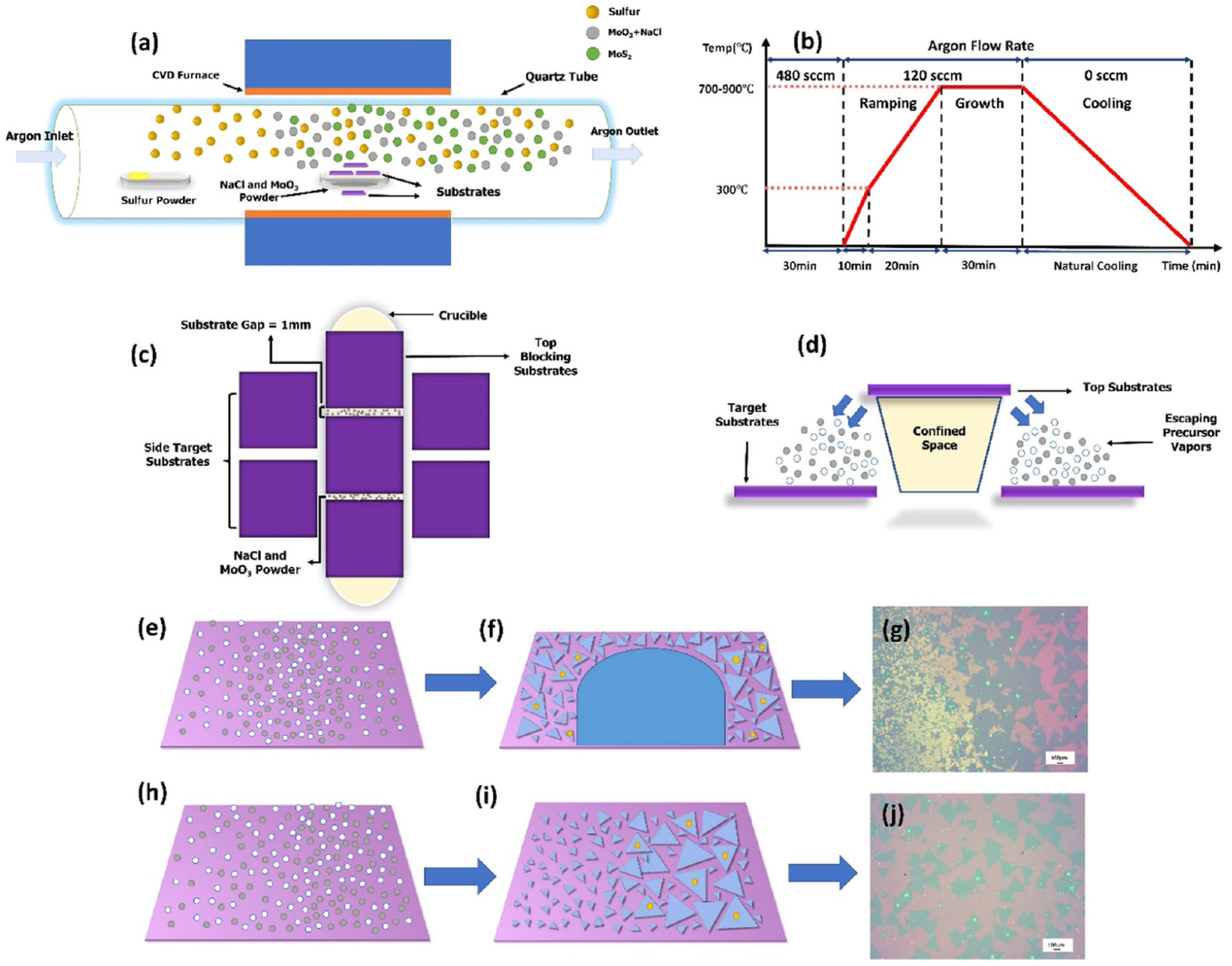

Figure 1. (a) Schematic of the CVD setup for MoS_2 growth and (b) the CVD growth parameters. (c) Top view of the placement of substrates on the top and sides of the crucible. (d) Side view of the schematic explaining escaping vapors from the crucible and their deposition on the target substrates. The growth on the top SiO_2 substrates: (e) Deposition of MoO_3 and NaCl vapors on the top substrate. (f) Sulfurization of nucleation sites in the middle of the substrate resulting in bulk MoS_2 growth in the middle and crystals around the edges. (g) OM image of the MoS_2 growth on the top substrate. Growth on SiO_2 substrates placed on the sides of the crucible: (h) Deposition of the MoO_3 and NaCl vapors on the target substrate, (i) sulfurization of nucleation sites resulting in the growth of large area MoS_2 crystals, and (j) OM morphology of the MoS_2 growth on the target substrate.

positive impact on the synthesis of 2D TMDC materials. The catalyst effect of NaCl on MoS_2 was discussed recently,[26] where both the positive and negative impacts of NaCl on MoS_2 growth were discussed. The role of concentration boundary layers on the CVD growth of MoS_2 using NaCl as the seeding promoter has been shown recently.[27] Through the control of the concentration boundary and optimization of parameters, the large-area growths of the monolayer, 2L, and 3L MoS_2 were demonstrated. The substrate-dependent, NaCl-assisted growth of MoS_2 was also discussed.[28] The demonstration of reduction in growth temperature was done along with the comparison of growth on various substrates. The formation of a water-soluble seeding layer is also discussed.

Moreover, the confined-space CVD method has proven to be an efficient method for the growth of 2D materials as it helps in the reduction of reactants concentration, stabilized growth conditions, and controllability of vapor flow. It ensures that the growth of 2D materials is of high quality where the uniformity of the grown 2D material is also maintained.[29] Similar methods have been deployed previously for attaining large-scale growth of graphene flakes such as the pita-pocket method[30] and the hole-pocket method,[31] in which high nucleation is controlled by regulating the adsorption and permeation of the gases used for synthesis. The confined-space CVD method has also been proven to be a better method for the growth of large-sized and clean MoS_2 crystals as the controlled flow of the precursor vapors is ensured.[32,33] There are several parameters which are involved in the growth of the MoS_2 crystals; these include substrate location, amount of precursor, precursor temperature, seeding promoters, growth pressure, carrier gas flow rate, and the growth time. Previously various studies have been conducted for the proper control of these parameters to obtain the desired MoS_2 crystal morphology.[34−36] However, an in-depth understanding of the MoS_2 synthesis through confined-space CVD at various temperatures and the addition of NaCl as a seeding promoter still needs exploration.

https://doi.org/10.1021/acsomega.2c03108
ACS Omega 2022, 7, 30074−30086

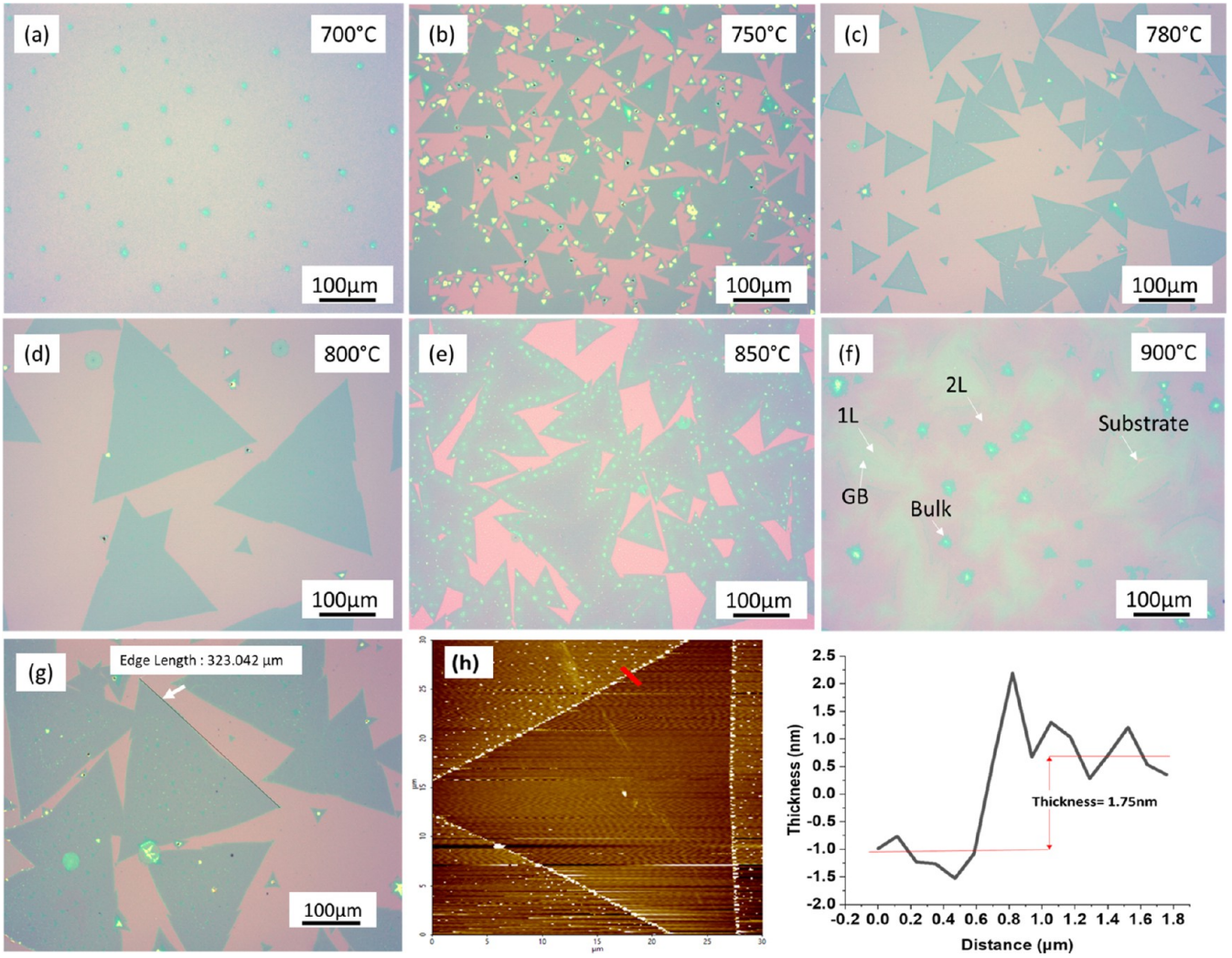

Figure 2. Changes in the morphology of MoS_2 crystals based on growth temperature. (a–f) Optical microscope images of MoS_2 grown on the SiO_2 substrate with temperature changing from 700 to 900 °C with 25 mg of NaCl and a MoO_3/S ratio of 1:20. (g) Edge length of a large-area MoS_2 flake grown at 800 °C. (h) AFM image and the line profile of monolayer MoS_2 crystal grown at a temperature of 780 °C.

In this work, we have adopted a new method for controllable growth of MoS_2 which amalgamates the NaCl-assisted growth with confined-space CVD. We demonstrate a systematic study for the large-scale controllable growth of highly crystalline MoS_2 crystals using the salt-assisted confined-space CVD method. The work explores the role of NaCl and growth temperature in the controllable growth of MoS_2. The work shows control over the number of layers of MoS_2 as well as over the morphology of grown MoS_2. Utilizing various techniques of characterization such as atomic force microscopy (AFM), optical microscopy (OM), Raman spectroscopy (Raman), scanning electron microscopy (SEM), X-ray photoelectron spectroscopy (XPS), and energy-dispersive X-ray spectroscopy (EDX), the analysis of the crystallinity, uniformity, and thickness of monolayer, bilayer and bulk MoS_2 crystals is done. Moreover, the electrical performance of the fabricated transistors shows promising results, which opens the gate for further applications of the CVD-grown MoS_2.

RESULTS AND DISCUSSION

Figure 1a shows the schematic of the confined-space CVD setup used for the growth of MoS_2. The confined space is created in the crucible when it is blocked with SiO_2/Si substrates from the top (Figure S4). The substrates placed on the outside of the crucible are the target substrates on which the escaping vapors from the crucible are deposited (Figure 1d). The size of both the blocking and target substrates is 1.5 × 1.5 cm^2. However, to ensure that some of the vapors actually escape the crucible, there are small gaps (1 mm) left in the blocking substrates that can act as an outlet for the precursor vapors (Figure 1c). A mixture of MoO_3 and NaCl was placed in a crucible in the middle of the furnace while the sulfur powder is placed on the upstream side (see Experimental Section). The growth conditions are shown in Figure 1b. Figure 1e–g shows the deposition of vaporized precursors on the top substrate. During the growth process of MoS_2 using the confined-space CVD, most of the vapors of the precursors in the main boat, NaCl and MoO_3, are blocked by the substrates placed directly on top of the boat. This results in the growth of nonuniform and bulk MoS_2 on the underside in the middle of the substrate. However, the diffusion of vapors results in the escape of some vapors from the gaps in the top substrates resulting in their deposition on the target substrates. As most of the vapors are blocked by the top substrates, the growth on the target substrates is relatively clean and uniform. The diffusion of vapors from the crucible and the presence of

https://doi.org/10.1021/acsomega.2c03108
ACS Omega 2022, 7, 30074–30086

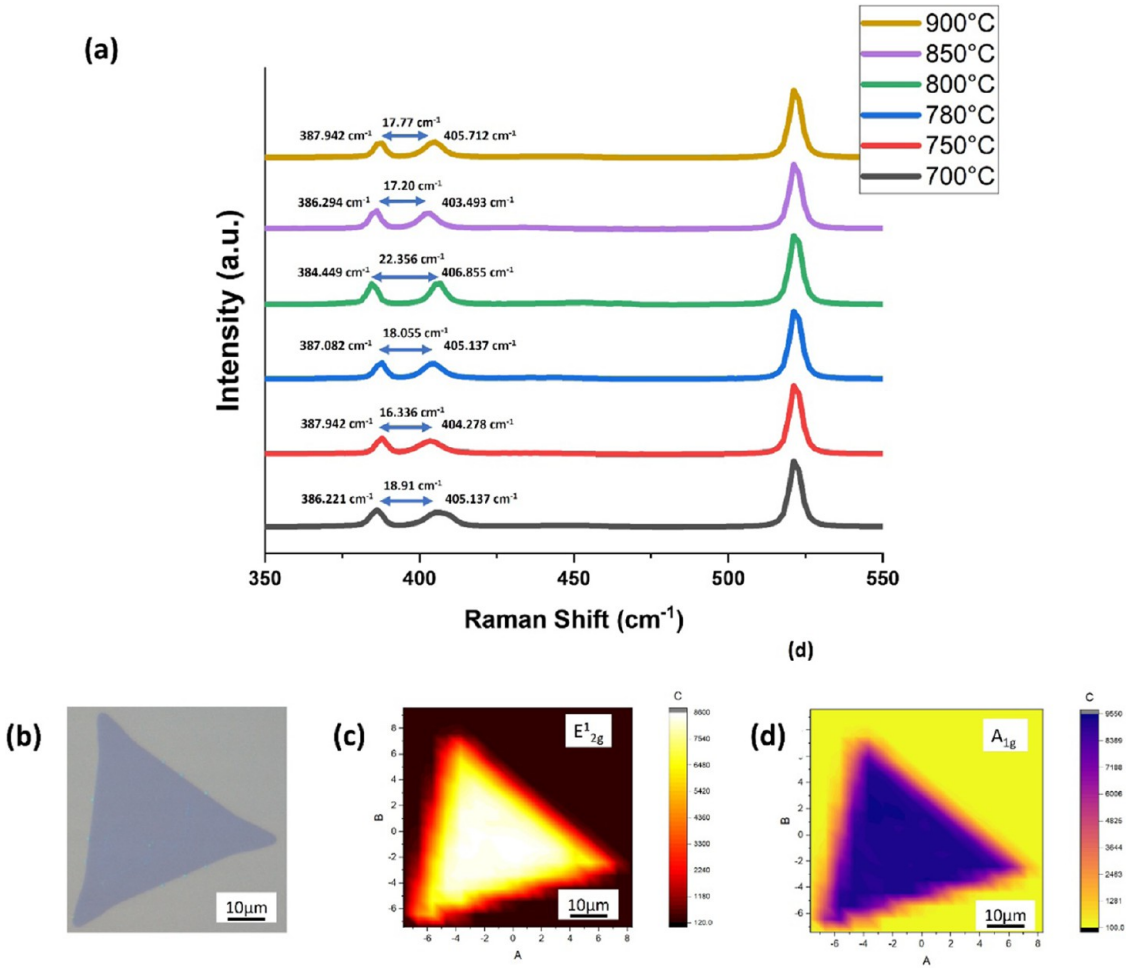

Figure 3. Raman spectra of MoS_2: (a) Comparison of the peak difference of MoS_2 grown at different temperatures. (b) OM image of a MoS_2 flake grown at 780 °C. (c, d) Raman intensity mapping of the E^1_{2g} and A_{1g} vibrational modes, respectively.

secondary substrates result in morphological variations of the grown MoS_2 crystals on the substrates.

For the target substrates, the region close to the crucible has a higher concentration of vapors, which results in high nucleation, as illustrated in Figure 1h–j. The size of the MoS_2 crystals is also bigger in this region. In the middle part of the substrate, the MoS_2 crystals are more distanced from one another. The size of these triangles also reduces as we move them away from the boat. In the region of the substrate near the boat, there is growth of large MoS_2 crystals, and the length of the crystals is found to be up to 300 μm, as shown in Figure 2. This shows the growth of conspicuously large crystals of MoS_2 comparable with the large-sized crystals that have been reported previously.[37]

We began by investigating the effect of temperature on the growth of large-area MoS_2 using a systematic study. The growth was carried out by placing the substrates at different temperatures between 700 and 900 °C while sulfur was kept in a low-temperature zone (150–180 °C), as shown in Figure 2a–f. All of the other experimental parameters were kept the same for these experiments (100 mg sulfur, 25 mg NaCl, and 5 mg MoO_3). For the characterization of MoS_2 grown at different temperatures, Raman spectroscopy was used to find the layer structure of MoS_2. The Raman signals of MoS_2 emerge in the forms of in-plane vibrational mode (referred to as E^1_{2g}) and out-of-plane vibrational mode (A_{1g}). The frequencies of these vibrational modes as well as the difference between the A_{1g} and E^1_{2g} modes can be used for the identification of the number of layers of MoS_2.[38] The positioning of the Raman modes depends on the layer thickness, impurities, and strain.[39,40] The Raman spectra were observed at the central region of the MoS_2 crystals grown at different temperatures, and it is observed that the crystals have high crystalline quality. The Raman spectra for growth at different temperatures representing the average peak difference are shown in Figure 3a, where no clear correlation was observed between the growth temperature and crystal thickness. The frequency values at E^1_{2g} and A_{1g} are also indicated for each case.

At 700 °C, the crystals of MoS_2 are small and barely visible under the optical microscope (Figure 2a). The optical microscope shows very small nanoparticles of MoS_2 grown at this temperature which indicates that this temperature is not ideal for the growth of large-area MoS_2 crystals. However, Raman peaks are still detected at this temperature where the characteristic E^1_{2g} and A_{1g} peaks are observed at 386.221 and 405.137 cm^{-1}, respectively. The peak difference "Δk" observed between the E^1_{2g} and A_{1g} modes is 18.916 cm^{-1}, which corresponds to monolayer MoS_2. For the temperature of 750 °C, large-scale monolayer MoS_2 crystals (Δk = 16.336 cm^{-1}) are grown along with bright small crystals of bulk MoS_2 (Δk = 24.073 cm^{-1}).[39] At 780 °C, large-scale monolayer MoS_2

https://doi.org/10.1021/acsomega.2c03108
ACS Omega 2022, 7, 30074–30086

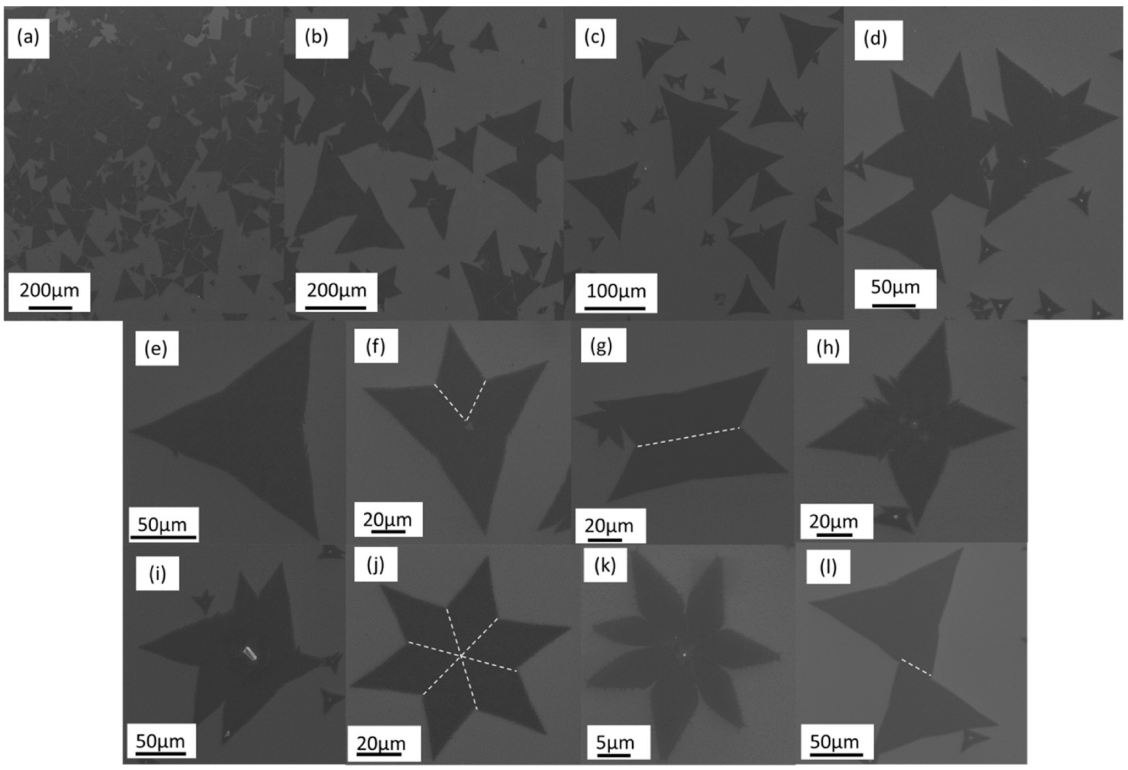

Figure 4. SEM images of MoS_2 crystals grown on SiO_2 substrate at a growth temperature of 780 °C with a MoO_3/S ratio of 1:20 and 25 mg NaCl. (a–d) SEM images of MoS_2 with low magnification. High-magnification SEM images of various shapes of CVD-grown MoS_2: (e) three-point star, (f) four-point star, (g) tilt boundary, (h) mirror boundary, (i, j) six-point star, (k) seven-point star, and (l) mirror twins.

crystals (Δk = 18.055 cm^{-1}) are observed with more clean and uniform growth. The frequency position values are 387.082 and 405.137 cm^{-1}. Both the modes indicate a blueshift. However, the blue shift for the E^1_{2g} mode is more significant, which results in a reduced Δk as compared to highly crystalline exfoliated MoS_2 flakes. This can be explained by the presence of thermally induced strain due to growth at high temperatures because of lattice mismatch between the layer and the substrate.[41] This result represents the optimum temperature of 780 °C for the growth of uniform and large-scale crystals of monolayer MoS_2, as shown in Figures 2c and S1c,d. The growth at 800 °C shows highly uniform large-scale bilayer MoS_2 crystals (Δk = 22.35 cm^{-1}) with the crystal edge length exceeding 300 μm (Figures 2g and S1b). Both the layers of MoS_2 are perfectly stacked on top of each other as the edges of both the crystals match perfectly. The growth of bilayer at this temperature can be associated with changes in sulfur evaporation rate.[42] At 850 °C, large-scale monolayer MoS_2 crystals (Δk = 17.20 cm^{-1}) are observed with roughness around the edges (Figure 2e). This roughness around the edges can be attributed to the nonuniform growth of the secondary layer on the edges of the crystal. The MoS_2 grown at 900 °C shows high coverage with secondary growth of MoS_2 on top (Figure 2f). The continuous layer has visible grain boundaries, which is an indication of the merging of highly crystalline and large crystals of MoS_2 through chemical bonding. As the large-area monolayer grains of MoS_2 merge together, the process of in-plane growth stops and a second layer starts to grow on top of the first layer with van der Waals adhesion forming a layer-by-layer structure. The Raman shift for the continuous layer (1L), the secondary flake (2L), and the bright spot in the middle (bulk) was found to be 17.77, 22.356, and 24.073 cm^{-1}, respectively.[43] For confirming the thickness of the grown MoS_2 crystal at various temperatures, AFM was used (Figure S3). The topography image and its thickness profile of monolayer flakes grown at 780 °C are shown in Figure 2h. The thickness observed is 1.75 nm, which corresponds to bilayer MoS_2. However, the Raman spectroscopy reveals the thickness to be monolayer (Δk = 18.055 cm^{-1}) corresponding to 0.8 nm thickness. The contradiction in the thickness measurement can be explained by errors in the AFM height measurement that are induced by surface roughness, impurities, background noise, thermal vibrations induced by the cantilever, and the difference in the interacting forces depending on the samples.[44−46] The uniformity of the grown crystals was also determined using Raman mapping for the same growth conditions. The Raman maps were obtained for both the vibrating modes E^1_{2g} and A_{1g}, as shown in Figure 3b–d. The Raman mapping indicates that the flake is uniform and has high crystallinity.[47]

This dependency of MoS_2 growth on temperature can be explained with the help of diffusion rates of Mo, S, and NaCl at elevated temperatures. The diffusion rate and the deposition of the MoO_3, sulfur, and NaCl vapors on the substrate surface vary with the change in temperature. For the growth at a lower temperature, the MoO_3 clusters that are deposited on the surface of the substrate have a lower concentration and small size. This results in an ease of reduction of the MoO_3 cluster into the MoS_2 clusters at the beginning of the growth process. Thus, the formation of 2D nuclei on the surface of the substrate occurs. The further continuation of the growth process results in an increase in the domain size, and the MoS_2 domains are created with both the monolayer and bilayer structures. In the case of growth at elevated temperatures, the

https://doi.org/10.1021/acsomega.2c03108
ACS Omega 2022, 7, 30074−30086

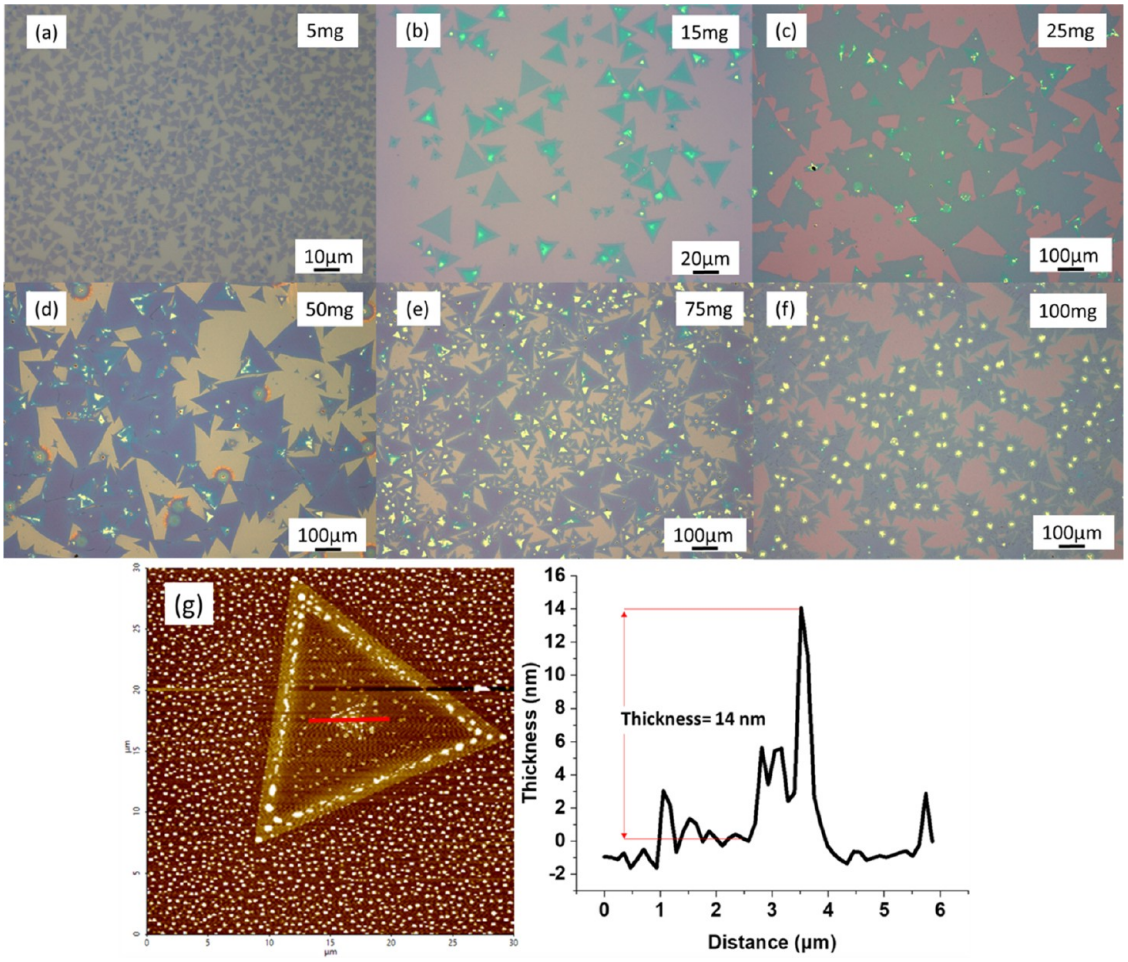

Figure 5. Changes in the morphology of MoS_2 crystals based on the amount of NaCl. (a–f) Optical microscopic images of MoS_2 grown on a SiO_2 substrate with the NaCl amount changing from 5 to 100 mg with a MoO_3/S ratio of 1:20 at a growth temperature of 780 °C. (g) The AFM topography shows the thickness of these bright spots around 14 nm.

high diffusion rate of the precursors results in the transport of a high concentration of nanoparticles on the surface of the substrate. This results in rapid sulfurization and growth of the MoS_2 crystals with the deposition of multilayer nuclei of the $MoO_{3-x}S_y$ nanoparticles.

The role of NaCl is also crucial at higher temperatures as the metal oxides have more tendency to react with molten NaCl at higher temperatures. This results in a higher vapor pressure of the metal precursors, and the reaction rate is also promoted. The further growth of these nanoparticles induces the growth of larger MoS_2 crystals.[48,49] However, this trend is not observed as the temperature increases indefinitely. As the temperature is increased beyond 780 °C, the flake size and the tendency for the growth of multilayer crystals increases. The high diffusion of precursors due to high temperatures increases the population of the nucleation sites, limiting the areas for the grains to grow.[50] However, the growth at higher temperatures results in more coverage on the substrates with a higher rate for growth of multilayers of MoS_2.

The growth process indicates the evolution of the shapes of MoS_2. For better understanding of the surface morphology of the MoS_2 crystals, scanning electron microscopy (SEM) was used. The SEM images show various shapes depending on different growth conditions, as shown in Figure 4. All of the structures in Figure 4 show clear edges of the grains with different angles, indicating the polycrystalline nature of these samples.[51] This shape evolution can be explained by the change in the local concentration of Mo and S precursors due to the confined-space CVD approach. The structure of the grown MoS_2 is dependent on the distance of the substrate from the source because of the difference of the Mo/S ratio. It is also observed that the growth at higher temperatures (850–900 °C) indirectly promotes the shape evolution of the MoS_2 crystals. This can be attributed to changes in the vapor concentration of Mo and S depending on the growth temperature as the growth rate of the zigzag edges for S and Mo varies.[52] These types of edge terminations are normally observed in the MoS_2 crystals, and the high reactivity of these terminations results in the growth from these edges instead of the basal plane of MoS_2. The structures having the shape of three-point stars are usually single crystals. Depending on the rate of growth of different crystal edges, the shape of the crystal is determined. As there are various shapes that have been observed on the substrates in this work, it can be established that the changes in the shape evolution is observed because of the variation in the Mo/S ratio and temperature. The reduction rate of MoO_3 varies depending on the temperature, resulting in the change in Mo proportion as compared to S.[36] The SEM images in Figure 4e–n show the growth of simple triangular-shaped crystals, three-point star, four-point star, six-point star, and twin crystals with representative grain boundaries. The formation of complicated morphologies like

https://doi.org/10.1021/acsomega.2c03108
ACS Omega 2022, 7, 30074–30086

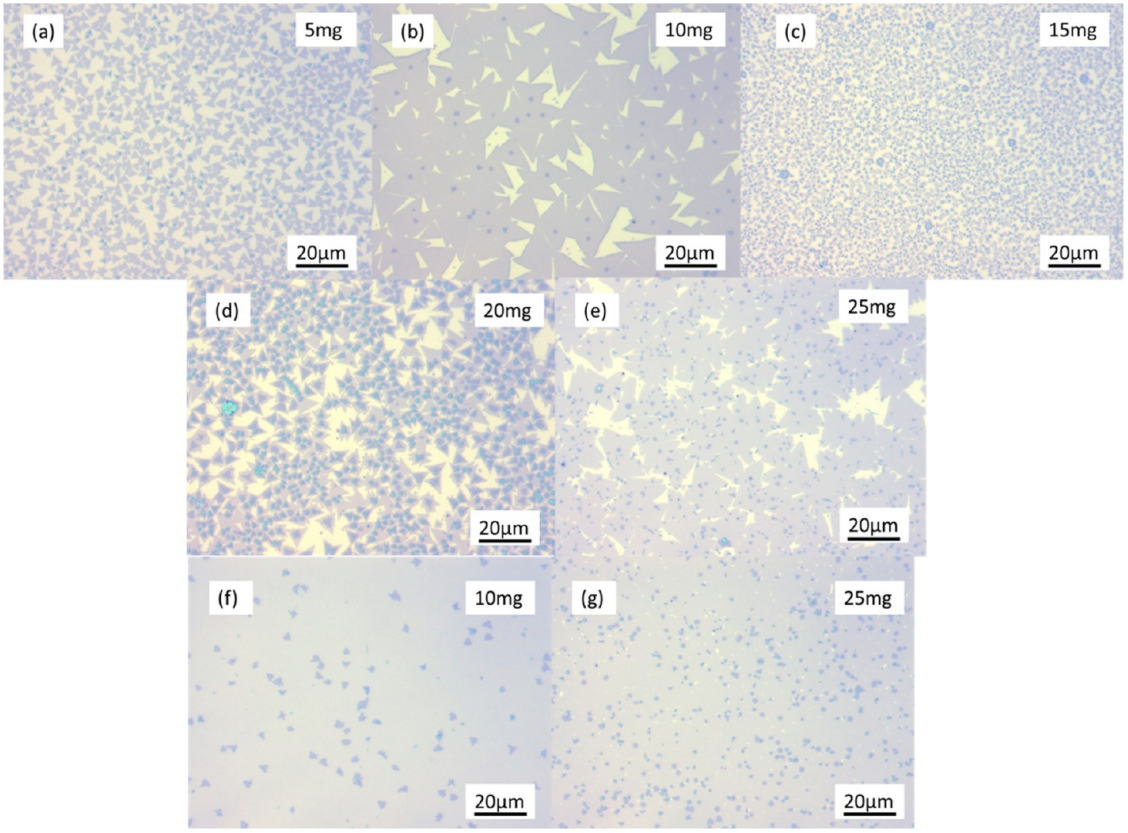

Figure 6. Changes in the morphology of MoS_2 crystals based on the MoO_3/S ratio. Optical microscope images of MoS_2 grown on SiO_2 substrate at a temperature of 780 °C with sulfur = 100 mg and NaCl = 25 mg and MoO_3 (a) 5 mg, (b) 10 mg, (c) 15 mg, (d) 20 mg, and (e) 25 mg. Formation of continuous layer at selected area on the substrates with MoO_3 amounts (f) 10 mg and (g) 25 mg.

the six-point star (Figure 4f,j) can be explained by the merging of two misoriented grains with different kinetics of growth.[53] The presence of cyclic twins (Figure 4k) is attributed to the symmetric intergrowth of two or more crystals.[54] The formation of mirror boundary (Figure 4g) is also observed which occurs due to the intersection of two MoS_2 flakes with 180° relative in-plane rotation.[52,55]

Based on the findings of the above experiments, we have identified 780 °C to be the optimal temperature for the growth of large-area MoS_2 monolayers. Figure 5 demonstrates the changes in the MoS_2 morphology by changes in the amount of NaCl. The experiments are performed by changing the amount of NaCl from 5 to 100 mg with a MoO_3/S ratio of 1:20 at a growth temperature of 780 °C. Figure 5a−f shows how the crystal morphology is related to the amount of NaCl. With the NaCl amount of 5 mg, the growth of small-sized monolayer MoS_2 crystals is observed, which corresponds to insufficient availability of NaCl for reaction kinetics. However, the growth at these conditions is highly uniform with high coverage. With the increase in the amount of NaCl to 15 mg, there is a clear increase in the size of MoS_2 crystals as the crystals having edges longer than 20 μm are observed. However, nonuniformity can be observed in the grown flakes of MoS_2 as there is presence of 1L, 2L, 3L, and bulk MoS_2 crystals. As the NaCl is increased up to 25 mg, there is a clear observation of an increase in the flake size as crystals with edge lengths greater than 200 μm are observed. This condition results in the growth of highly uniform monolayer crystals of MoS_2. Further increase in the amount of NaCl causes larger particles in the nucleation sites, which results in the bulk growth of MoS_2 (yellow spot), and bulk and monolayer MoS_2 crystals tend to grow with a large size distribution, as observed in Figure 5d−f.

NaCl plays a very important role as a seeding promoter in the growth of MoS_2. The metal halides like NaCl have the tendency for evaporation at a lower temperature than the metal oxides as they are highly active.[56] The mixture of MoO_3 and NaCl powders results in the formation of a molten solution at growth temperatures. As NaCl has higher vapor pressure, this results in the increased vaporization of both NaCl and MoO_3, which promotes nucleation at low growth temperatures.

The main reason behind the role of NaCl is the presence of Na in the compound. This deposited Na acts as a catalyst and accelerates the growth rate.[57] This is achieved by the lowering of the energy barrier to grow MoS_2.[58] NaCl results in the formation of intermediates like NaO between Na and O on the surface of the SiO_2 substrate.[28,59] At the start of the growth process, these NaO bonds enhance the growth rate by lowering the energy barrier.[58] However, as the growth time increases, the saturation of NaO bonds on the surface causes reduction of the surface energy and thus, the growth rate. The reduced surface energy also promotes the growth of multilayer MoS_2 as the stacking behavior of crystals is preferred in this case.[60] The change in the reaction kinetics is also clear from the changes in the shape of MoS_2 at a higher NaCl concentration (Figure 5d−f).

There is also an observation of clusters of bulk MoS_2 (Figure S1a) that are formed on the surface of the substrate as the NaCl-assisted growth takes place. The role of NaCl in the formation of cluster-like structures can be confirmed using NaCl separately in the same crucible without mixing it with the

https://doi.org/10.1021/acsomega.2c03108
ACS Omega 2022, 7, 30074−30086

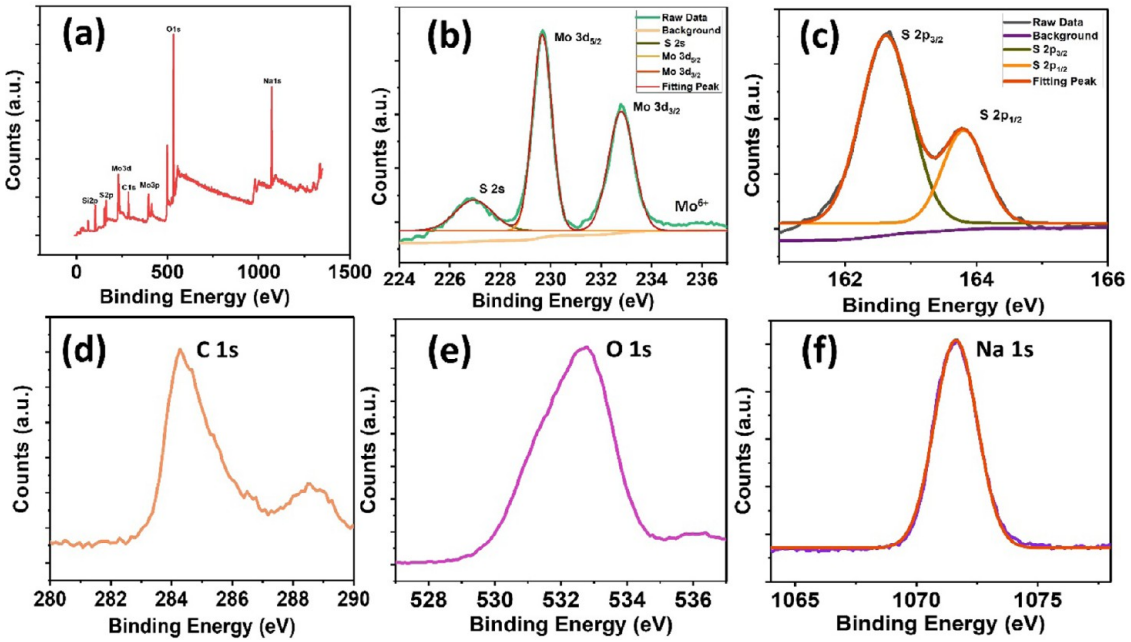

Figure 7. XPS analysis of MoS_2 grown at 780 °C: (a) XPS survey. (b) Peaks for Mo 3d orbitals $3d_{5/2}$ and $3d_{3/2}$ at 229.68 and 232.80 eV, respectively. Sulfur oxidation peak at 226.99 eV. A peak of low intensity observed at 235.98 eV representing MoO_3. (c) Orbitals of S 2p, $2p_{3/2}$ and $2p_{1/2}$, observed at 162.62 and 163.80 eV, respectively. (d) Carbon calibration peak at 284.28 eV. (e) O 1s peak at 532.78 eV representing the oxide layer of the Si substrate. (f) Na 1s peak observed at 1071.69 eV representing $Na_2Mo_xO_x$ or Na_2SO_4.

MoO_3 precursor. This method results in the formation of huge nucleation sites suggesting that large vapors of NaCl are deposited on the substrate. This causes the stacking of MoS_2 crystals on top of one another forming a cluster of bright yellow spots. The thickness of these clusters is confirmed by Raman spectroscopy, and the results suggest that there are multiple layers of MoS_2 which are stacked above one another. This suggests that the presence of NaCl might result in the formation of different morphologies depending on the synthesis parameters. It is also observed that for higher concentration of NaCl, bright yellow spots are observed in the center of the grown crystals. When the thickness of these bright spots was observed using AFM, it was found to be around 14 nm, as shown in Figure 5g. This indicates the presence of multilayer MoS_2. On the other hand, the yellow spot formation on the growth substrate can be attributed to the presence of large clusters of MoO_3 ($MoO_{3-x}S_y$ clusters), which are not sulfurized properly.[48]

The presence of $MoO_{3-x}S_y$ nanoparticles can be confirmed by XPS data. As shown in Figure 7b, the low-intensity peak observed at 235.98 eV shows the presence of MoO_3 on the substrate. Moreover, the EDX analysis was carried out on the yellow spot for further confirmation (Figure S5). The analysis shows significant presence of oxygen along with Mo, S, and Na (Table S1), indicating the presence of $MoO_{3-x}S_y$ clusters.

Based on the study conducted on the amount of NaCl, 5 mg is identified to be the optimum amount for high coverage of the monolayer having the tendency of forming a continuous layer (Figure 5a). Further optimization of the precursor ratio was performed to obtain a continuous monolayer on the substrate. Figure 6a−e show the changes in the morphology of the grown MoS_2 by changing the concentration of MoO_3 at optimum conditions of NaCl and temperature for high coverage (5 mg and 780 °C) while all of the other growth parameters were kept the same. The results were evaluated by keeping the sulfur at 100 mg and changing the concentration of MoO_3 from 5 to 25 mg with a step size of 5 mg. This results in the formation of small-sized monolayer crystals of MoS_2 on the target substrate, as shown in Figure 6a−e. The crystals formed on the edges of the top substrate are comparatively large and are shown in Figure S2.

The small size of the crystals found in Figure 5a was already attributed to the reduced concentration of NaCl (5 mg), which results in moderate nucleation on the substrate with high coverage. The part of the substrate near the boat gets more input of nucleation vapors resulting in the merging of MoS_2 to form a partial continuous layer on some portion of the substrate, as shown in Figure 6f,g. This also results in the formation of a locally continuous layer on the substrate. However, with high coverage of the substrate, some secondary nucleation sites are found, which appear in the form of small crystals of MoS_2 (Figure 6f,g). The thickness of the continuous monolayer was confirmed using Raman spectroscopy, showing the distance between the two peaks to be 15.47 cm^{-1}.

As a result, by comparing the different growth methods, i.e., growth at different temperatures, changing the amount of NaCl and MoO_3, the size, coverage, and thickness of the MoS_2 crystals can be controlled. The high coverage of monolayer MoS_2 can be achieved at a high growth temperature with a clear definition of grain boundaries indicating highly crystalline growth, in comparison with the continuous layer achieved by varying the MoO_3 concentration. However, this method has a disadvantage of the growth of large-size secondary flakes of MoS_2. It is also noted that the continuous layer was achieved in each case by optimizing the precursor ratios without extending the growth time, which shows that our proposed methodology can be adopted for changing the substrate coverage with the same growth time (30 min).

For a better understanding of the atomic structure of the grown MoS_2, its chemical properties, and to investigate the role

https://doi.org/10.1021/acsomega.2c03108
ACS Omega 2022, 7, 30074−30086

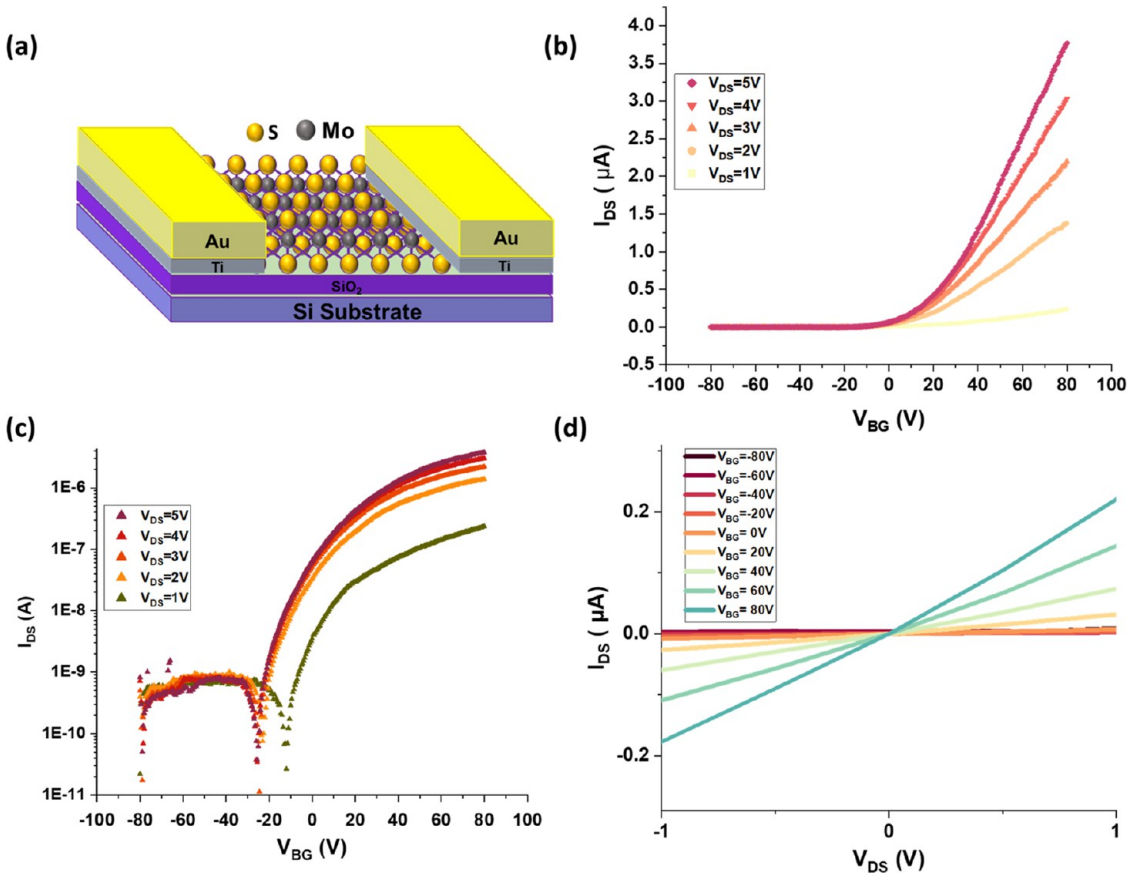

Figure 8. (a) Schematic of the fabricated MoS_2 FETs. (b, c) Transfer curves at different values of V_{DS}. (d) Characteristic curve (I_{DS}−V_{DS}) of 2D MoS_2-based FET at different back-gate voltages (V_{BG}).

of NaCl, we carried out XPS analysis of the MoS_2 crystals grown at 780 °C (Figure 7). The survey spectrum of MoS_2 can be observed in Figure 7a. Figure 7b shows binding energy (BE) peaks at 229.68 and 232.80 eV, which correspond to the $3d_{5/2}$ and $3d_{3/2}$ orbitals of Mo^{4+}, which is representative of the molybdenum in its charged state in MoS_2.[61] There is also an observation of low intensity peak at 235.98 eV. This corresponds to the presence of oxides of Mo likely MoO_3, which might be due do the presence of the unreacted precursor of MoO_3, which is usually observed in CVD-grown MoS_2 as Mo^{6+} peaks.[61−63] The Mo^{4+} $3d_{5/2}$ has the absorption peak, which is located at 226.99 eV; this can be attributed to the oxidation of sulfur. The spin−orbit doublets for the S 2p spectrum are observed at the positions of 162.62 and 163.80 eV, which shows the BE for $2p_{3/2}$ and $2p_{1/2}$, respectively, as shown in Figure 7c. The energy separation for these peaks is observed to be 1.18 eV. Figure 7d represents the BE of C 1s peak, which as observed at 284.28 eV for the purpose of calibration. Figure 7e shows the BE of the O 1s peak, which is centered at 532.78 eV and might be due to the oxide layer on the Si substrate. The presence of the core-level spectra of Na 1s is also observed at 1071.69 eV (Figure 7f), which arises due to the presence of Na. This shows that the Na from NaCl might be present beneath the crystals in the form of growth intermediates like $Na_2Mo_xO_x$[26] and Na_2SO_4.[28]

To evaluate the quality of the CVD-grown MoS_2, back-gate field-effect transistors (FETs) were fabricated with two terminals on monolayer MoS_2, as shown in Figure 8a. The measurements were carried out under ambient conditions to evaluate the ON/OFF ratio, carrier mobilities, and the on-state currents.

The transfer curves for V_{DS} = 1−5 V are plotted in linear and log scales, as shown in Figure 8b,c. The device exhibits a strong n-type behavior, as it achieves on-state at the positive gate voltage. The I−V curves show symmetric and linear behaviors measured at different back-gate voltages (sweeping from −80 to 80 V), as represented in Figure 8d. This confirms that the contact at the interface of Ti/MoS_2 is ohmic in nature as explained by Fermi-level pinning.[64] The devices exhibited an ON/OFF ratio of up to 10^5, which is better than the previously reported values for CVD-grown MoS_2[65,66] and comparable with the other previous reports.[67,68] We have also estimated the field-effect mobility of the monolayer MoS_2 devices for various channel lengths, from the transfer curve using the equation

$$\mu = \frac{L}{W}\frac{\delta I_{DS}}{\delta V_{BG}}\frac{1}{C_{oxide}V_{DS}} \quad (1)$$

where L and W denote the channel length and channel width, respectively, I_{DS} is the current between the drain and the source terminal, C_{oxide} is the capacitance of the gate dielectric, and V_{DS} is the applied drain-to-source voltage. The apparent value of mobility for our devices lies between 0.6 and 1.9 cm^2 V^{-1} s^{-1}, which is in accordance with the previously reported range (0.1−10 cm^2 V^{-1} s^{-1}) of values for exfoliated as well as CVD-grown MoS_2.[58,65,69−71] The mobility of the devices can be improved further with the use of top-gate electrodes with high-k dielectrics. The usage of NaCl as a seeding promoter

https://doi.org/10.1021/acsomega.2c03108
ACS Omega 2022, 7, 30074−30086

and surface impurities might also degrade the device performance.[60] There is still some room for improvement in the device performance, which can be achieved through the optimization of growth parameters and better electrode fabrication. The performance of device gives a clear indication that the method of synthesis reported here is a feasible method for the growth of monolayer to few-layer MoS_2 for FET applications.

CONCLUSIONS

This work illustrates the use of different methodologies for the growth of MoS_2 on a large scale using a confined-space CVD method with NaCl as a seeding promoter. The experiments conducted illustrate the control of important growth parameters like temperature, precursor ratio, and the amount of NaCl for yielding highly crystalline MoS_2 with varying morphologies. The characterization of the grown MoS_2 is carried out using optical microscopy, scanning electron microscopy (SEM), Raman spectroscopy, AFM, XPS, and EDX analysis. The work also sheds light on the proposed explanation for the growth of large-scale MoS_2 crystals on the substrate with different morphologies by the variation in growth conditions and its electrical properties. The method suggested in this article can be utilized for the controlled growth of other transition-metal dichalcogenides with different morphologies, which can be used for the fabrication of different electronic devices.

EXPERIMENTAL SECTION

CVD Growth of MoS_2. The preparation of MoS_2 crystals in this work was performed using a confined-space CVD method. SiO_2 (300 nm)/Si was used as the growth substrate, which was placed in a high temperature zone in the CVD chamber. MoO_3 powder (≥99.5%, Sigma-Aldrich) and NaCl were mixed in an alumina boat and placed in the center of the furnace in the high temperature zone. A quartz boat containing sulfur powder (≥99.5%, Sigma-Aldrich) was placed upstream in a lower-temperature zone with temperature around (150−180 °C). Before the growth process, the pressure in the furnace was reduced to 1.5×10^{-2} Torr and purging was carried out inside the tube with Ar (99.99% purity) at 500 sccm to remove any preexisting contaminants. The SiO_2/Si substrate was cut into a square shape with the dimensions 1.5 × 1.5 cm^2. The substrates were cleaned using deionized water, acetone, and isopropyl alcohol (IPA) for 10 min each and was dried with nitrogen gas. The substrates were placed on top of the boat as well as on the sides of the boat containing the MoO_3 precursor. The blocking substrates were placed at a distance of 1 mm from each other to ensure that a small outlet is created for escaping vapors. During the growth process, Ar (99.99% purity) gas was used as a carrier gas at 120 sccm. First the system was ramped up to a temperature of 300 °C in 10 min. Then, the temperature was ramped up from 300 to 700−900 °C in 20 min. The system was maintained at the growth temperature for 30 min and then allowed to cool down naturally.

Device Fabrication and Characterizations. MoS_2 FET devices were fabricated directly on the growth substrate without transferring. The thickness of the grown flake was identified using AFM and Raman measurements. The drain and source electrodes were defined on the crystals using standard photolithography and e-beam lithography process followed by the deposition of Ti (10 nm)/Au (40 nm) through e-beam evaporator system. The deposited samples were then soaked in acetone for lift-off process and cleaned using IPA and deionized water, followed by drying with N_2 gas. The devices were then thermally annealed at a temperature of 200 °C for 2 h in the presence of argon at 20 sccm for reducing the contact resistance and to remove any interfacial adsorbates. The measurements of the FET device were carried using a parameter analyzer (Keithley 4200A-SCS).

ASSOCIATED CONTENT

Supporting Information

The Supporting Information is available free of charge at https://pubs.acs.org/doi/10.1021/acsomega.2c03108.

Optical microscope images of large MoS_2 crystals (Figure S1); optical microscope images of large MoS_2 crystals grown on the top substrate (Figure S2); AFM topography (Figure S3); confined-space CVD setup (Figure S4); energy-dispersive X-ray analysis (EDX) (Figure S5) (PDF)

AUTHOR INFORMATION

Corresponding Author

Yongho Seo − *Department of Nanotechnology and Advanced Materials Engineering, and HMC, Sejong University, 05006 Seoul, South Korea;* orcid.org/0000-0002-5695-5493; Email: yseo@sejong.ac.kr

Authors

Muhammad Suleman − *Department of Nanotechnology and Advanced Materials Engineering, and HMC, Sejong University, 05006 Seoul, South Korea;* orcid.org/0000-0002-8317-7236

Sohee Lee − *Department of Nanotechnology and Advanced Materials Engineering, and HMC, Sejong University, 05006 Seoul, South Korea;* orcid.org/0000-0002-7866-3811

Minwook Kim − *Department of Nanotechnology and Advanced Materials Engineering, and HMC, Sejong University, 05006 Seoul, South Korea;* orcid.org/0000-0001-9408-0256

Van Huy Nguyen − *Department of Nanotechnology and Advanced Materials Engineering, and HMC, Sejong University, 05006 Seoul, South Korea;* orcid.org/0000-0003-4651-9679

Muhammad Riaz − *Department of Nanotechnology and Advanced Materials Engineering, and HMC, Sejong University, 05006 Seoul, South Korea*

Naila Nasir − *Department of Nanotechnology and Advanced Materials Engineering, and HMC, Sejong University, 05006 Seoul, South Korea*

Sunil Kumar − *Department of Nanotechnology and Advanced Materials Engineering, and HMC, Sejong University, 05006 Seoul, South Korea;* orcid.org/0000-0001-9429-3809

Hyun Min Park − *Department of Nanotechnology and Advanced Materials Engineering, and HMC, Sejong University, 05006 Seoul, South Korea;* orcid.org/0000-0003-0570-3306

Jongwan Jung − *Department of Nanotechnology and Advanced Materials Engineering, and HMC, Sejong University, 05006 Seoul, South Korea;* orcid.org/0000-0002-1397-212X

Complete contact information is available at:

https://doi.org/10.1021/acsomega.2c03108
ACS Omega 2022, 7, 30074−30086

https://pubs.acs.org/10.1021/acsomega.2c03108

Author Contributions

M.S. and Y.S. designed and processed the experimental data, performed the analysis, and drafted the manuscript. M.S. worked on the CVD growth, device fabrication, Raman spectroscopy, and scanning electron microscopy. L.S. contributed to CVD growth and aided in results interpretation. M.K. performed the AFM measurement. M.R. and J.J. contributed to the device fabrication and FET measurements. V.H.N. contributed to device fabrication. H.M.P. contributed to the XPS measurement. S.K. contributed to the EDX analysis. N.N. designed the figures. All of the authors discussed the results and commented on the manuscript.

Notes

The authors declare no competing financial interest.

■ ACKNOWLEDGMENTS

This research was supported by a National Research Foundation of Korea (NRF) grant funded by the Korea government (MSIT) (NRF-2020R1A6A1A03043435 and 2020R1A2C1099862). Also, this research was supported by the Korea Institute for Advancement of Technology (KIAT) grant funded by the Korea government (MOTIE) (P0012451, The Competency Development Program for Industry Specialist).

■ REFERENCES

(1) Cho, H.; Kang, D.; Lee, Y.; Bae, H.; Hong, S.; Cho, Y.; Kim, K.; Yi, Y.; Park, J. H.; Im, S. Dramatic Reduction of Contact Resistance via Ultrathin LiF in Two-Dimensional MoS2 Field Effect Transistors. *Nano Lett.* **2021**, *21*, 3503−3510.

(2) Liu, X.; Hu, S.; Lin, Z.; Li, X.; Song, L.; Yu, W.; Wang, Q.; He, W. High-performance MoS2 photodetectors prepared using a patterned gallium nitride substrate. *ACS Appl. Mater. Interfaces* **2021**, *13*, 15820−15826.

(3) Wang, L.; Zou, X.; Lin, J.; Jiang, J.; Liu, Y.; Liu, X.; Zhao, X.; Liu, Y. F.; Ho, J. C.; Liao, L. Perovskite/black phosphorus/MoS2 photogate reversed photodiodes with ultrahigh light on/off ratio and fast response. *ACS Nano* **2019**, *13*, 4804−4813.

(4) Singh, E.; Kim, K. S.; Yeom, G. Y.; Nalwa, H. S. Atomically thin-layered molybdenum disulfide (MoS2) for bulk-heterojunction solar cells. *ACS Appl. Mater. Interfaces* **2017**, *9*, 3223−3245.

(5) Luo, X.; Peng, Z.; Wang, Z.; Dong, M. Layer-by-Layer Growth of AA-Stacking MoS2 for Tunable Broadband Phototransistors. *ACS Appl. Mater. Interfaces* **2021**, *13*, 59154−59163.

(6) Joseph, S.; Thomas, S.; Mohan, J.; Kumar, A. S.; Jayasree, S. T.; Thomas, S.; Kalarikkal, N. Theoretical study on tuning band gap and electronic properties of atomically thin nanostructured MoS2/metal cluster heterostructures. *ACS Omega* **2021**, *6*, 6623−6628.

(7) Chu, T.; Ilatikhameneh, H.; Klimeck, G.; Rahman, R.; Chen, Z. Electrically tunable bandgaps in bilayer MoS2. *Nano Lett.* **2015**, *15*, 8000−8007.

(8) Cho, U.; Kim, S.; Shin, C. Y.; Song, I. Tabletop Fabrication of High-Performance MoS2 Field-Effect Transistors. *ACS Omega* **2022**, *24*, 21220−21224.

(9) Chen, Y.; Deng, W.; Chen, X.; Wu, Y.; Shi, J.; Zheng, J.; Chu, F.; Liu, B.; An, B.; You, C. Carrier mobility tuning of MoS2 by strain engineering in CVD growth process. *Nano Res.* **2021**, *14*, 2314−2320.

(10) Cho, C.; Wong, J.; Taqieddin, A.; Biswas, S.; Aluru, N. R.; Nam, S.; Atwater, H. A. Highly strain-tunable interlayer excitons in MoS2/WSe2 heterobilayers. *Nano Lett.* **2021**, *21*, 3956−3964.

(11) McClellan, C. J.; Yalon, E.; Smithe, K. K.; Suryavanshi, S. V.; Pop, E. High Current Density in Monolayer MoS2 Doped by AlO x. *ACS Nano* **2021**, *15*, 1587−1596.

(12) Bandaru, N.; Kumar, R. S.; Sneed, D.; Tschauner, O.; Baker, J.; Antonio, D.; Luo, S.-N.; Hartmann, T.; Zhao, Y.; Venkat, R. Effect of pressure and temperature on structural stability of MoS2. *J. Phys. Chem. C* **2014**, *118*, 3230−3235.

(13) Kumar, A.; Yagodkin, D.; Stetzuhn, N.; Kovalchuk, S.; Melnikov, A.; Elliott, P.; Sharma, S.; Gahl, C.; Bolotin, K. I. Spin/Valley Coupled Dynamics of Electrons and Holes at the MoS2−MoSe2 Interface. *Nano Lett.* **2021**, *21*, 7123−7130.

(14) Goswami, T.; Rani, R.; Hazra, K. S.; Ghosh, H. N. Ultrafast carrier dynamics of the exciton and trion in MoS2 monolayers followed by dissociation dynamics in Au@ MoS2 2D heterointerfaces. *J. Phys. Chem. A* **2019**, *10*, 3057−3063.

(15) Liu, J.-B.; Hu, J.-Y.; Liu, C.; Tan, Y.-M.; Peng, X.; Zhang, Y. Mechanically exfoliated MoS2 nanosheets decorated with SnS2 nanoparticles for high-stability gas sensors at room temperature. *Rare Met.* **2021**, *40*, 1536−1544.

(16) Muratore, C.; Hu, J.; Wang, B.; Haque, M. A.; Bultman, J. E.; Jespersen, M. L.; Shamberger, P.; McConney, M.; Naguy, R.; Voevodin, A. Continuous ultra-thin MoS2 films grown by low-temperature physical vapor deposition. *Appl. Phys. Lett.* **2014**, *104*, No. 261604.

(17) Pondick, J. V.; Woods, J. M.; Xing, J.; Zhou, Y.; Cha, J. J. Stepwise sulfurization from MoO3 to MoS2 via chemical vapor deposition. *ACS Appl. Nano Mater.* **2018**, *1*, 5655−5661.

(18) Jawaid, A.; Nepal, D.; Park, K.; Jespersen, M.; Qualley, A.; Mirau, P.; Drummy, L. F.; Vaia, R. A. Mechanism for liquid phase exfoliation of MoS2. *Chem. Mater.* **2016**, *28*, 337−348.

(19) Ding, W.; Hu, L.; Dai, J.; Tang, X.; Wei, R.; Sheng, Z.; Liang, C.; Shao, D.; Song, W.; Liu, Q. Highly ambient-stable 1T-MoS2 and 1T-WS2 by hydrothermal synthesis under high magnetic fields. *ACS Nano* **2019**, *13*, 1694−1702.

(20) Li, L.; Long, R.; Prezhdo, O. V. Why chemical vapor deposition grown MoS2 samples outperform physical vapor deposition samples: time-domain ab initio analysis. *Nano Lett.* **2018**, *18*, 4008−4014.

(21) Ahn, C.; Park, Y.; Shin, S.; Ahn, J.-G.; Song, I.; An, Y.; Jung, J.; Kim, C. S.; Kim, J. H.; Bang, J. Growth of Monolayer and Multilayer MoS2 Films by Selection of Growth Mode: Two Pathways via Chemisorption and Physisorption of an Inorganic Molecular Precursor. *ACS Appl. Mater. Interfaces* **2021**, *13*, 6805−6812.

(22) Wang, X.; Feng, H.; Wu, Y.; Jiao, L. Controlled synthesis of highly crystalline MoS2 flakes by chemical vapor deposition. *J. Am. Chem. Soc.* **2013**, *135*, 5304−5307.

(23) Jeon, J.; Jang, S. K.; Jeon, S. M.; Yoo, G.; Jang, Y. H.; Park, J.-H.; Lee, S. Layer-controlled CVD growth of large-area two-dimensional MoS 2 films. *Nanoscale* **2015**, *7*, 1688−1695.

(24) Chen, F.; Jiang, X.; Shao, J.; Lu, B.; Fu, L.; Zhao, S.; Su, W. Space-confined CVD growth of 2D-MoS 2 crystals with tunable dimensionality via adjusting growth conditions. *CrystEngComm* **2021**, *23*, 1345−1351.

(25) Ling, X.; Lee, Y.-H.; Lin, Y.; Fang, W.; Yu, L.; Dresselhaus, M. S.; Kong, J. Role of the seeding promoter in MoS2 growth by chemical vapor deposition. *Nano Lett.* **2014**, *14*, 464−472.

(26) Chen, L.; Zang, L.; Chen, L.; Wu, J.; Jiang, C.; Song, J. Study on the catalyst effect of NaCl on MoS 2 growth in a chemical vapor deposition process. *CrystEngComm* **2021**, *23*, 5337−5344.

(27) Singh, A.; Sharma, M.; Singh, R. NaCl-Assisted CVD Growth of Large-Area High-Quality Trilayer MoS2 and the Role of the Concentration Boundary Layer. *Cryst. Growth Des.* **2021**, *21*, 4940−4946.

(28) Singh, A.; Moun, M.; Sharma, M.; Barman, A.; Kapoor, A. K.; Singh, R. NaCl-assisted substrate dependent 2D planar nucleated growth of MoS2. *Appl. Surf. Sci.* **2021**, *538*, No. 148201.

(29) Zhou, S.; Wang, R.; Han, J.; Wang, D.; Li, H.; Gan, L.; Zhai, T. Ultrathin non-van der Waals magnetic Rhombohedral Cr2S3: space-confined chemical vapor deposition synthesis and raman scattering investigation. *Adv. Funct. Mater.* **2019**, *29*, No. 1805880.

(30) Li, X.; Magnuson, C. W.; Venugopal, A.; Tromp, R. M.; Hannon, J. B.; Vogel, E. M.; Colombo, L.; Ruoff, R. S. Large-area graphene single crystals grown by low-pressure chemical vapor

https://doi.org/10.1021/acsomega.2c03108
ACS Omega 2022, 7, 30074−30086

deposition of methane on copper. *J. Am. Chem. Soc.* **2011**, *133*, 2816−2819.
(31) DanháPhan, H.; NgocáHuynh, V. Large-area single-crystal graphene grown on a recrystallized Cu (111) surface by using a hole-pocket method. *Nanoscale* **2016**, *8*, 13781−13789.
(32) Zhang, X.; Huangfu, L.; Gu, Z.; Xiao, S.; Zhou, J.; Nan, H.; Gu, X.; Ostrikov, K. Controllable Epitaxial Growth of Large-Area MoS2/WS2 Vertical Heterostructures by Confined-Space Chemical Vapor Deposition. *Small* **2021**, *17*, No. 2007312.
(33) Zhang, J.; Qian, Y.; Nan, H.; Gu, X.; Xiao, S. Large-scale MoS2 (1− x) Se2x monolayers synthesized by confined-space CVD. *Nanotechnology* **2021**, *32*, No. 355601.
(34) Chen, F.; Su, W. The effect of the experimental parameters on the growth of MoS 2 flakes. *CrystEngComm* **2018**, *20*, 4823−4830.
(35) Özden, A.; Ay, F.; Sevik, C.; Perkgöz, N. K. CVD growth of monolayer MoS2: Role of growth zone configuration and precursors ratio. *Jpn. J. Appl. Phys.* **2017**, *56*, No. 06GG05.
(36) Yang, S. Y.; Shim, G. W.; Seo, S.-B.; Choi, S.-Y. Effective shape-controlled growth of monolayer MoS2 flakes by powder-based chemical vapor deposition. *Nano Res.* **2017**, *10*, 255−262.
(37) Chen, J.; Tang, W.; Tian, B.; Liu, B.; Zhao, X.; Liu, Y.; Ren, T.; Liu, W.; Geng, D.; Jeong, H. Y. Chemical vapor deposition of high-quality large-sized MoS2 crystals on silicon dioxide substrates. *Adv. Sci.* **2016**, *3*, No. 1500033.
(38) Li, H.; Zhang, Q.; Yap, C. C. R.; Tay, B. K.; Edwin, T. H. T.; Olivier, A.; Baillargeat, D. From bulk to monolayer MoS2: evolution of Raman scattering. *Adv. Funct. Mater.* **2012**, *22*, 1385−1390.
(39) Kumar, V. K.; Dhar, S.; Choudhury, T. H.; Shivashankar, S.; Raghavan, S. A predictive approach to CVD of crystalline layers of TMDs: the case of MoS 2. *Nanoscale* **2015**, *7*, 7802−7810.
(40) Chae, W. H.; Cain, J. D.; Hanson, E. D.; Murthy, A. A.; Dravid, V. P. Substrate-induced strain and charge doping in CVD-grown monolayer MoS2. *Appl. Phys. Lett.* **2017**, *111*, No. 143106.
(41) Luo, S.; Cullen, C. P.; Guo, G.; Zhong, J.; Duesberg, G. S. Investigation of growth-induced strain in monolayer MoS2 grown by chemical vapor deposition. *Appl. Surf. Sci.* **2020**, *508*, No. 145126.
(42) Zobel, A.; Boson, A.; Wilson, P. M.; Muratov, D. S.; Kuznetsov, D. V.; Sinitskii, A. Chemical vapour deposition and characterization of uniform bilayer and trilayer MoS 2 crystals. *J. Mater. Chem. C* **2016**, *4*, 11081−11087.
(43) Ji, J.; Zhang, A.; Fan, J.; Li, Y.; Wang, X.; Zhang, J.; Plummer, E.; Zhang, Q. Giant magneto-optical Raman effect in a layered transition metal compound. *Proc. Natl. Acad. Sci.* **2016**, *113*, 2349−2353.
(44) Ruggeri, F. S.; Šneideris, T.; Vendruscolo, M.; Knowles, T. P. Atomic force microscopy for single molecule characterisation of protein aggregation. *Arch. Biochem. Biophys.* **2019**, *664*, 134−148.
(45) Lee, H.; Lee, N.; Seo, Y.; Eom, J.; Lee, S. Comparison of frictional forces on graphene and graphite. *Nanotechnology* **2009**, *20*, No. 325701.
(46) Amani, M.; Chin, M. L.; Birdwell, A. G.; O'Regan, T. P.; Najmaei, S.; Liu, Z.; Ajayan, P. M.; Lou, J.; Dubey, M. Electrical performance of monolayer MoS2 field-effect transistors prepared by chemical vapor deposition. *Appl. Phys. Lett.* **2013**, *102*, No. 193107.
(47) Chiawchan, T.; Ramamoorthy, H.; Buapan, K.; Somphonsane, R. CVD Synthesis of Intermediate State-Free, Large-Area and Continuous MoS2 via Single-Step Vapor-Phase Sulfurization of MoO2 Precursor. *Nanomaterials* **2021**, *11*, No. 2642.
(48) Zhou, D.; Shu, H.; Hu, C.; Jiang, L.; Liang, P.; Chen, X. Unveiling the growth mechanism of MoS2 with chemical vapor deposition: from two-dimensional planar nucleation to self-seeding nucleation. *Cryst. Growth Des.* **2018**, *18*, 1012−1019.
(49) Zhou, J.; Lin, J.; Huang, X.; Zhou, Y.; Chen, Y.; Xia, J.; Wang, H.; Xie, Y.; Yu, H.; Lei, J. A library of atomically thin metal chalcogenides. *Nature* **2018**, *556*, 355−359.
(50) Zhou, H.; Wang, C.; Shaw, J. C.; Cheng, R.; Chen, Y.; Huang, X.; Liu, Y.; Weiss, N. O.; Lin, Z.; Huang, Y. Large area growth and electrical properties of p-type WSe2 atomic layers. *Nano Lett.* **2015**, *15*, 709−713.
(51) Zheng, W.; Qiu, Y.; Feng, W.; Chen, J.; Yang, H.; Wu, S.; Jia, D.; Zhou, Y.; Hu, P. Controlled growth of six-point stars MoS2 by chemical vapor deposition and its shape evolution mechanism. *Nanotechnology* **2017**, *28*, No. 395601.
(52) Wang, S.; Rong, Y.; Fan, Y.; Pacios, M.; Bhaskaran, H.; He, K.; Warner, J. H. Shape evolution of monolayer MoS2 crystals grown by chemical vapor deposition. *Chem. Mater.* **2014**, *26*, 6371−6379.
(53) Chen, S.; Gao, J.; Srinivasan, B. M.; Zhang, G.; Yang, M.; Chai, J.; Wang, S.; Chi, D.; Zhang, Y.-W. Revealing the grain boundary formation mechanism and kinetics during polycrystalline MoS2 growth. *ACS Appl. Mater. Interfaces* **2019**, *11*, 46090−46100.
(54) Zhang, H.; Ha, D.-H.; Hovden, R.; Kourkoutis, L. F.; Robinson, R. D. Controlled synthesis of uniform cobalt phosphide hyper-branched nanocrystals using tri-n-octylphosphine oxide as a phosphorus source. *Nano Lett.* **2011**, *11*, 188−197.
(55) Papanai, G. S.; Pal, S.; Pal, P.; Yadav, B. S.; Garg, P.; Gupta, S.; Ansari, S.; Gupta, B. K. New insight into the growth of monolayer MoS 2 flakes using an indigenously developed CVD setup: a study on shape evolution and spectroscopy. *Mater. Chem. Front.* **2021**, *5*, 5429−5441.
(56) Mobin, M.; Malik, A.; Ahmad, S. High temperature interactions of metal oxides with NaCl. *J. Less-Common Met.* **1990**, *160*, 1−14.
(57) Shi, Y.; Yang, P.; Jiang, S.; Zhang, Z.; Huan, Y.; Xie, C.; Hong, M.; Shi, J.; Zhang, Y. Na-assisted fast growth of large single-crystal MoS2 on sapphire. *Nanotechnology* **2018**, *30*, No. 034002.
(58) Yang, P.; Zou, X.; Zhang, Z.; Hong, M.; Shi, J.; Chen, S.; Shu, J.; Zhao, L.; Jiang, S.; Zhou, X. Batch production of 6-inch uniform monolayer molybdenum disulfide catalyzed by sodium in glass. *Nat. Commun.* **2018**, *9*, No. 979.
(59) Wang, Z.; Xie, Y.; Wang, H.; Wu, R.; Nan, T.; Zhan, Y.; Sun, J.; Jiang, T.; Zhao, Y.; Lei, Y. NaCl-assisted one-step growth of MoS2−WS2 in-plane heterostructures. *Nanotechnology* **2017**, *28*, No. 325602.
(60) Zhang, K.; Bersch, B. M.; Zhang, F.; Briggs, N. C.; Subramanian, S.; Xu, K.; Chubarov, M.; Wang, K.; Lerach, J. O.; Redwing, J. M. Considerations for utilizing sodium chloride in epitaxial molybdenum disulfide. *ACS Appl. Mater. Interfaces* **2018**, *10*, 40831−40837.
(61) Kim, I. S.; Sangwan, V. K.; Jariwala, D.; Wood, J. D.; Park, S.; Chen, K.-S.; Shi, F.; Ruiz-Zepeda, F.; Ponce, A.; Jose-Yacaman, M. Influence of stoichiometry on the optical and electrical properties of chemical vapor deposition derived MoS2. *ACS Nano* **2014**, *8*, 10551−10558.
(62) Kalanyan, B.; Kimes, W. A.; Beams, R.; Stranick, S. J.; Garratt, E.; Kalish, I.; Davydov, A. V.; Kanjolia, R. K.; Maslar, J. E. Rapid wafer-scale growth of polycrystalline 2H-MoS2 by pulsed metal−organic chemical vapor deposition. *Chem. Mater.* **2017**, *29*, 6279−6288.
(63) Syari'ati, A.; Kumar, S.; Zahid, A.; El Yumin, A. A.; Ye, J.; Rudolf, P. Photoemission spectroscopy study of structural defects in molybdenum disulfide (MoS 2) grown by chemical vapor deposition (CVD). *Chem. Commun.* **2019**, *55*, 10384−10387.
(64) Kim, C.; Moon, I.; Lee, D.; Choi, M. S.; Ahmed, F.; Nam, S.; Cho, Y.; Shin, H.-J.; Park, S.; Yoo, W. J. Fermi level pinning at electrical metal contacts of monolayer molybdenum dichalcogenides. *ACS Nano* **2017**, *11*, 1588−1596.
(65) Lee, Y. H.; Zhang, X. Q.; Zhang, W.; Chang, M. T.; Lin, C. T.; Chang, K. D.; Yu, Y. C.; Wang, J. T. W.; Chang, C. S.; Li, L. J. Synthesis of large-area MoS2 atomic layers with chemical vapor deposition. *Adv. Mater.* **2012**, *24*, 2320−2325.
(66) Şar, H.; Özden, A.; Yorulmaz, B.; Sevik, C.; Kosku Perkgoz, N.; Ay, F. A comparative device performance assesment of CVD grown MoS2 and WS2 monolayers. *J. Mater. Sci. Mater.* **2018**, *29*, 8785−8792.
(67) Tao, L.; Chen, K.; Chen, Z.; Chen, W.; Gui, X.; Chen, H.; Li, X.; Xu, J.-B. Centimeter-scale CVD growth of highly crystalline single-layer MoS2 film with spatial homogeneity and the visualization of grain boundaries. *ACS Appl. Mater. Interfaces* **2017**, *9*, 12073−12081.
(68) Yang, P.; Zhang, S.; Pan, S.; Tang, B.; Liang, Y.; Zhao, X.; Zhang, Z.; Shi, J.; Huan, Y.; Shi, Y. Epitaxial growth of centimeter-

https://doi.org/10.1021/acsomega.2c03108
ACS Omega 2022, 7, 30074−30086

scale single-crystal MoS2 monolayer on Au (111). *ACS Nano* **2020**, *14*, 5036−5045.
(69) Durairaj, S.; Krishnamoorthy, P.; Raveendran, N.; Ryu, B. D.; Hong, C.-H.; Seo, T. H.; Chandramohan, S. Barrier-assisted vapor phase CVD of large-area MoS 2 monolayers with high spatial homogeneity. *Nanoscale Adv.* **2020**, *2*, 4106−4116.
(70) Liu, B.; Chen, L.; Liu, G.; Abbas, A. N.; Fathi, M.; Zhou, C. High-performance chemical sensing using Schottky-contacted chemical vapor deposition grown monolayer MoS2 transistors. *ACS Nano* **2014**, *8*, 5304−5314.
(71) Lee, Y.-H.; Yu, L.; Wang, H.; Fang, W.; Ling, X.; Shi, Y.; Lin, C.-T.; Huang, J.-K.; Chang, M.-T.; Chang, C.-S. Synthesis and transfer of single-layer transition metal disulfides on diverse surfaces. *Nano Lett.* **2013**, *13*, 1852−1857.

https://doi.org/10.1021/acsomega.2c03108
ACS Omega 2022, 7, 30074−30086